ISBN: 978-3-95450-261-5 ISSN: 2673-7000 doi: 10.18429/JACoW-NAPAC2025-WEP016

DEMONSTRATION OF A SHEET ELECTRON BEAM PRODUCTION FROM A UNCD FIELD EMITTER ARRAY*

W. Choi†, D. Kim, H. Andrews, C.-C. Chang, M. Zuboraj, E. I. Simakov
Los Alamos National Laboratory, Los Alamos, NM, USA

Abstract

We used nitrogen-doped ultra-nanocrystalline diamonds to fabricate field emitter arrays and demonstrate production of a sheet electron beam. Diamond cathodes in the form of arrays of 1 by 81 pyramids were fabricated and tested at 20 kV. Beam images were recorded at several distances from a grid anode and used to estimate beam sizes. We found that the beam divergence angles are 0.23° in x direction, and 1.2° in y direction. There were a few obstacles during the experiments such as nonuniform emission and grid patterns in the beam images. They will be addressed in the future.

INTRODUCTION

Ultra-nanocrystalline diamond (UNCD) is a promising material for field emitters because of its mechanical and chemical stability, high thermal conductivity, and low electrical resistivity [1, 2]. UNCD deposited on flat surfaces can serve as a field emitter with its very small grain size. However, making a field emitter array (FEA) with a pyramid shape offers advantages, as it facilitates the characterization of beam emission area and emission properties. In addition, the pyramid shape reduces turn-on voltage for field emission from the arrays. A diamond field emitter array (DFEA) can be fabricated using conventional thin-film techniques, including Si-mold transfer, nanodiamond deposition via chemical vapor deposition (CVD), and brazing [3].

FEAs are widely used to realize cold cathodes which have several advantages over traditional thermionic and photo cathodes. The cold cathodes utilize field emission; therefore they don't require heating and laser systems. DFEAs are capable of operating under poor vacuum condition ($> 10^{-5}$ Torr) due to their high resistance to contamination and inherently low outgassing features [4]. Electron sources employing a cold cathode are compact, which can be essential for realizing table-top accelerators, dielectric laser accelerators, terahertz vacuum tubes, and more [5, 6].

We attempt to make sheet electron beams (SEBs) using DFEAs. SEBs are typically shaped like ellipses or rectangles that can be easily fabricated with DFEAs. Because of its shape, an SEB is capable of carrying more beam current than a conventional pencil beam. Also, an SEB with high aspect ratio can efficiently interact with planar structures.

We proposed to demonstrate fabrication of a special shaped field emitter array to produce an SEB for high frequency vacuum tubes. At Los Alamos, we established a field emitter array test stand where we can apply voltages up to a negative 40 kV to test field emitter arrays in a vacuum level of 10^{-7} Torr or lower. At this test stand, we can take beam images, measure beam current and study beam divergence. We fabricated diamond cathodes in the form of arrays of 1 by 81 pyramids and used them to demonstrate production of an SEB.

FABRICATION OF A DFEA

Fabrication process of a DFEA is illustrated in Fig. 1. Starting with dry oxidation of a Si wafer, the desired array of emitters is written using electron beam lithography with multi-pass method to draw precise patterns. A layer of SiO_2 is developed and subsequently removed using inductively coupled plasma etching. The exposed Si layer is further etched using tetramethylammonium hydroxide, an anisotropic etchant, resulting in the formation of inverted pyramidal structures. Then, a layer of UNCD is deposited on top of the Si layer using a CVD machine. The diamond layer is brazed onto a molybdenum substrate, and the Si and SiO_2 layers are etched away. The fabricated DFEA cathode is thoroughly cleaned and characterized using scanning electron microscopy (SEM). More details in fabrication and deposition of UNCD can be found in [3].

To demonstrate the generation of an SEB from a DFEA, we fabricated a DFEA with an array of 1 by 81 pyramids. The base of the pyramids is 25 µm and the pitch of the array is 50 µm. SEM analysis revealed a few blunt and double tips;

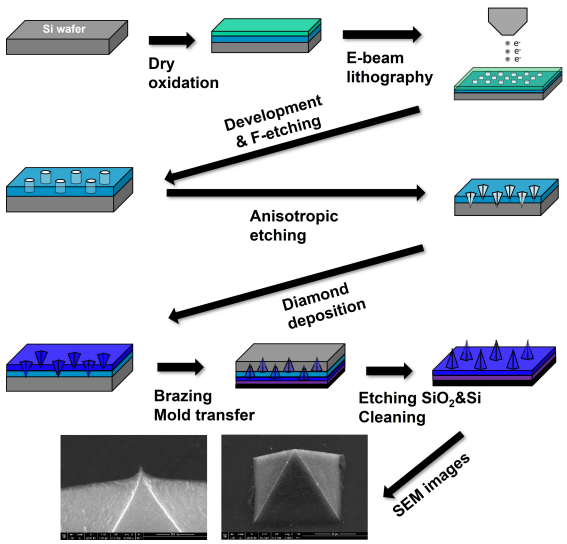

Figure 1: Overview of the fabrication process for DFEA.

* This work was supported by Los Alamos National Laboratory's Laboratory Directed Research and Development (LDRD) Program (20230110ER) and was performed, in part, at the Center for Integrated Nanotechnologies, an Office of Science User Facility operated for the U.S. Department of Energy (DOE) Office of Science.
† wonjin@lanl.gov

ISBN: 978-3-95450-261-5 ISSN: 2673-7000 doi: 10.18429/JACoW-NAPAC2025-WEP016

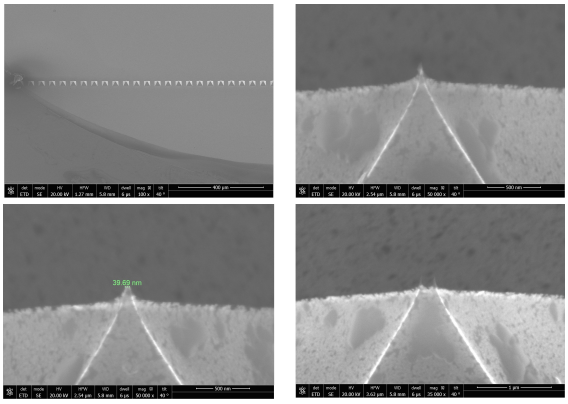

Figure 2: SEM images of the fabricated 1 by 81 DFEA cathode. (Top left) part of the array showing around 25 pyramids. (Top right) a single sharp tip. (Bottom left) a blunt tip with tip diameter of ~40 nm. (Bottom right) double sharp tips.

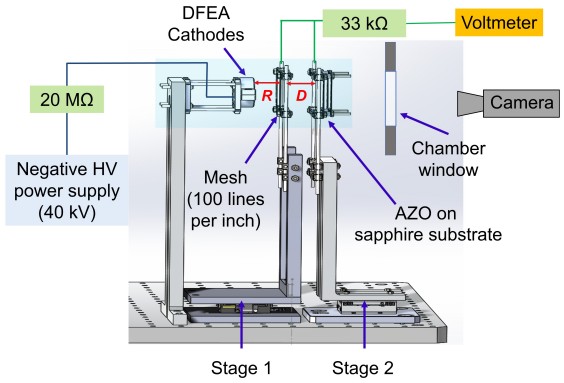

Figure 3: A schematic of the experimental setup.

however, the majority of the pyramidal structures exhibited single, sharp tips. The SEM images are shown in Fig. 2.

EXPERIMENTAL SETUP

For high voltage tests of the DFEA, we devised a setup depicted in Fig. 3, in a vacuum chamber. The chamber can maintain a vacuum pressure of 10^{-7} Torr or lower. The cathode is mounted on a fixed holder. A mesh grid anode and a screen are each mounted on independent motorized stages, allowing precise adjustment of the anode-cathode gap (R) and the grid-to-screen gap (D), as illustrated in Fig. 3. The diameter of a wire in the grid is 20 µm, and the pitch of the wires is 254 µm. A negative high voltage power supply that can provide more than 40 kV is used to generate electric field. The beam current is measured by converting the voltage in a 33 kΩ resistor. The screen is made of aluminum doped zinc oxide deposited on a sapphire substrate. Images on the screen are captured by a camera positioned outside the chamber.

We applied −20 kV at the DFEA cathode and grounded the grid and the screen. The cathode to grid gap is fixed at ~4 mm. While changing the grid-to-screen gap from 6.5 mm to 35 mm, we measured the beam current and took beam images.

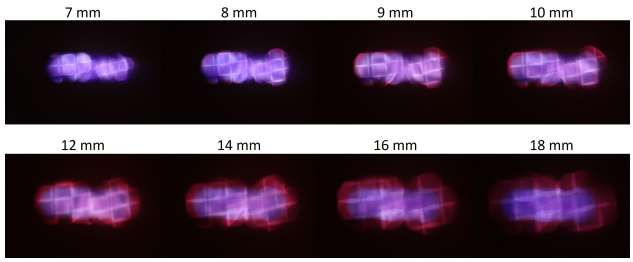

Figure 4: Beam images from 1 by 81 DFEA at several grid-to-screen distances.

ANALYSIS OF EXPERIMENTAL RESULT

The measured beam current varied from 5.5 µA to 7.3 µA during the test. While the variation is about ±14 %, space charge effect to trajectories of the emitted electrons should be negligible. The beam images taken at several grid-to-screen distances are shown in Fig. 4. It is obvious that the grid wires become brighter instead of making shadow on the screen. Our suspicion is that secondary electrons from the wires contribute some intensity and local electric field around the wires plays a role. We may use a grid with different material in the future. Another observation is that the color in the images change near beam edges starting at 8 mm. This is due to damages to the screen that occurred in previous tests. However, the damaged areas yield brighter pixels and therefore it is not a significant problem for our analysis. The test will be repeated later using a newly fabricated, undamaged screen.

2D Gaussian Fits of Beam Images

We fit a 2D Gaussian function to the beam images to estimate beam divergence in horizontal (x) and vertical (y) directions. The 2D Gaussian function used for fitting is defined as

$$f(x,y) = O + A\exp\left(-\left\{\left(\frac{\cos^2\theta}{2\sigma_x^2}+\frac{\sin^2\theta}{2\sigma_y^2}\right)(x-x_o)^2 + \left(\frac{\sin 2\theta}{2\sigma_x^2}-\frac{\sin 2\theta}{2\sigma_y^2}\right)(x-x_o)(y-y_o) + \left(\frac{\sin^2\theta}{2\sigma_x^2}+\frac{\cos^2\theta}{2\sigma_y^2}\right)(y-y_o)^2\right\}\right),$$

where σ_x and σ_y are spreads in x and y directions, θ is tilt angle, x_o, and y_o are centers, O is offset, and A is amplitude of the Gaussian.

Also, we used the beam images averaged by 6 images at each distance to minimize the effect of flickering pixels. The averaged beam images, as well as contours of the Gaussian fits, are shown in Fig. 5.

The σ_x and σ_y of the Gaussian fits are used to evaluate the beam sizes and beam divergences, and depicted in Fig. 6.

ISBN: 978-3-95450-261-5 ISSN: 2673-7000 doi: 10.18429/JACoW-NAPAC2025-WEP016

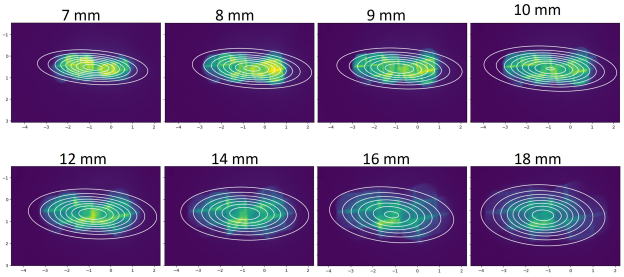

Figure 5: The averaged beam images and their Gaussian fits.

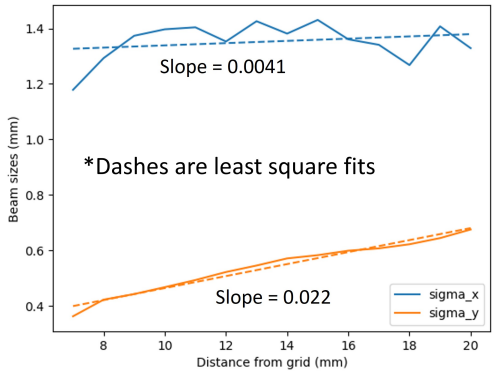

Figure 6: Evolution of beam sizes in x and y directions and their least square fits.

From the slopes of the least square fits of the beam sizes, beam divergence angles in x and y directions are estimated as 0.23° and 1.2°, respectively.

Higher divergence in the narrow dimension is a typical behavior of a space-charge-dominated SEB, which is not the case here. Since the array is arranged only over x direction, divergence of the beam in x direction is smaller. A simple statistic can show that the ratio of divergences in y and x directions are

$$\frac{db/dz}{da/dz} = \left(1 + \frac{M^2 - 1}{12}\frac{p^2}{b^2}\right)^{1/2} > 1,$$

where a, b are RMS beam sizes in x and y directions, p is the pitch of the array, and M is the number of tips. The divergence is therefore larger in y direction. With nominal parameters of $b = 0.6\,\text{mm}$, $M = 81$, and $p = 50\,\mu\text{m}$, the ratio is 2.19. Also, it should be noted that the errors in the Gaussian fits are relatively high, which can be evidenced by large fluctuation of σ_x in Fig. 6. Nonuniform emission, as well as the bright features of the grid wires are major causes of the errors. Also, the different tilt angles of each fit contribute to the fluctuation of σ_x.

Comparison with Simulation

A simulation was conducted using CST Particle Studio for comparison with the experimental data. In the simulation, the diameter of the emitting tips is set to 100 nm. We used unstructured tetrahedral meshes to manage vast difference in features (from nm scale to mm scale). Using particle data from the simulation, we estimated the same 2D Gaussian fits. Using maximum particle positions, the divergence angles are 5.4° and 2.9° in x and y directions, respectively. But RMS particle positions result in the divergence angles of 1.1° in x and 1.5° in y.

CONCLUSION

We fabricated a DFEA consisting of a 1 by 81 pyramids and successfully demonstrated production of an SEB. Several limitations remain, including nonuniform emission and the presence of grid patterns in the beam images. The nonuniform emission may be alleviated through improved fabrication techniques and cathode conditioning, whereas the origin of the grid patterns requires further investigation. Currently, the cathode is employed for low beam current testing. Future work will focus on estimating beam emittance in both transverse directions using a pepper-pot method, followed by high beam current evaluations.

REFERENCES

[1] A. V. Sumant, O. Auciello, R. W. Carpick, S. Srinivasan, and J. E. Butler, "Ultrananocrystalline and nanocrystalline diamond thin films for MEMS/NEMS applications", *MRS Bulletin*, vol. 35, no. 4, pp. 281–288, 2010. doi:10.1557/mrs2010.550

[2] O. Auciello and A. V. Sumant, "Status review of the science and technology of ultrananocrystalline diamond (UNCD™) films and application to multifunctional devices", *Diamond and Related Materials*, vol. 19, no. 7, pp. 699–718, 2010. doi:10.1016/j.diamond.2010.03.015

[3] D. Kim, H. L. Andrews, B. K. Choi, and E. I. Simakov, "Fabrication of micron-scale diamond field emitter arrays for dielectric laser accelerators", in *2018 IEEE Advanced Accelerator Concepts Workshop (AAC)*, pp. 1–3, 2018. doi:10.1109/AAC.2018.8659407

[4] J. D. Jarvis *et al.*, "Fabrication of Diamond Field-Emitter-Array Cathodes for Free-Electron Lasers", in *Proc. FEL'08*, Gyeongju, Korea, Aug. 2008, pp. 269–270. https://jacow.org/FEL2008/papers/TUPPH016.pdf

[5] K. L. Jensen, "Field emitter arrays for plasma and microwave source applications", *Physics of Plasmas*, vol. 6, no. 5, pp. 2241–2253, 1999. doi:10.1063/1.873502

[6] C. Huang *et al.*, "Physics of Electron Beam Generation and Dynamics From Diamond Field Emitter Arrays", in *Proc. IPAC'19*, Melbourne, Australia, May 2019, pp. 2137–2139. doi:10.18429/JACoW-IPAC2019-TUPTS091